Beyond average Hamiltonian theory for quantum sensing

Jner Tzern Oon,[1,2,*,†] Sebastian C. Carrasco,[3,*] Connor A. Hart,[2] George A. Witt,[1]
Vladimir S. Malinovsky,[3] and Ronald Walsworth[1,2,4]

[1]*Department of Physics, University of Maryland, College Park, Maryland 20742, USA*
[2]*Quantum Technology Center, University of Maryland, College Park, Maryland 20742, USA*
[3]*DEVCOM Army Research Laboratory, Adelphi, Maryland 20783, USA*
[4]*Department of Electrical and Computer Engineering, University of Maryland, College Park, Maryland 20742, USA*

(Received 10 October 2024; revised 12 September 2025; accepted 15 January 2026; published 26 February 2026)

The Magnus expansion underpins average Hamiltonian theory (AHT), a central tool in quantum control and sensing that is used to generate efficient approximations of system dynamics. Here, we demonstrate that the conditions for Magnus expansion convergence are violated under typical operating regimes for sensing using solid-state spin systems. We also establish that certain symmetries, such as those found in rapid echo pulse sequences, cancel all higher-order Magnus terms outside standard convergence frameworks. We introduce an exact method to compute the sensor response beyond the AHT regime, and apply it to both broadband and narrow-band magnetometry protocols. Our results clarify AHT limits and enable opportunities in pulse sequence design through symmetry-driven convergence, with implications for entanglement-enhanced sensing and quantum Fisher information estimation in control protocols.

DOI: 10.1103/w2sf-zxdk

I. INTRODUCTION

The Magnus expansion provides a general framework for solving nonautonomous linear differential equations involving linear operators [1] and has become a foundational tool across physics, for example, in classical mechanics [2], quantum field theory [3], and atomic physics [4–6]. Given its widespread use, a clear understanding of the conditions under which the Magnus expansion converges is critical for both theoretical predictions and experimental control [7].

A prominent application of the Magnus expansion comes in the form of average Hamiltonian theory (AHT) [8], first developed in the context of nuclear magnetic resonance (NMR) [9,10]. AHT approximates time evolution using an effective time-independent Hamiltonian obtained using the Magnus expansion [1]. Beyond its perturbative accuracy, AHT preserves Hermiticity at any truncation order and often captures qualitative physical properties of the system dynamics [11]. Besides prolific use in the development of pulse sequences for spin-spin interactions, AHT is a powerful tool for both analytical and numerical predictions of closed quantum dynamics [12–15]. Its experimental implementation typically involves resonant radiofrequency, microwave, or optical driving of internal quantum (e.g., spin) states.

In recent years, AHT has played an increasingly central role in quantum sensing, where it has been applied both for semiquantitative analysis of dynamical decoupling protocols [16,17] and as a basis for pulse sequence design in strongly interacting systems [18–20]. For example, AHT has enabled experimental advances in dynamical decoupling and magnetic field sensing for dense nitrogen-vacancy (NV) center ensembles [21,22].

Here, we identify a crucial limitation of quantum sensing applications of AHT: The conditions that guarantee Magnus expansion convergence are routinely violated by experimental operating regimes for solid-state magnetometry—even in the absence of interactions. This fundamental constraint challenges the validity of AHT in practical sensing applications.

However, we also demonstrate that specific pulse symmetries can restore Magnus expansion accuracy beyond standard convergence pathways involving algebraic and operator nilpotency [6,7,23,24]. In particular, we analytically show that a recently developed rapid echo sequence [25] cancels all higher-order Magnus terms, offering a symmetry-based solution to an open problem in pulse sequence design [23]. Further, we introduce an exact method for computing sensor responses to classical target fields, applicable beyond the AHT regime. We illustrate this method on widely used pulse sequences for both broadband (dc) and narrow-band (ac) magnetometry.

Our results reveal insights into entanglement-enhanced sensing, by combining rapid echo structure and our exact calculation of sensor response. First, we identify an equivalence between a squeezing echo sequence [26,27] and a nonlinear interferometer with a two-axis countertwisting Hamiltonian [28]. Second, we show that AHT convergence enables

[*]These authors contributed equally to this work.
[†]Contact author: jjoon@umd.edu

efficient evaluation of the quantum Fisher information (QFI), a key figure of merit used to benchmark entangled input states for control and sensing protocols [29]. As constructed, these results generalize to arbitrary Hamiltonians, opening directions for design principles and searches for hidden symmetries that stabilize AHT convergence under practical conditions.

II. AVERAGE HAMILTONIAN THEORY

To describe a general pulse sequence applied to a quantum system, we consider a series of n control pulses with unitary operators $P_1, \dots, P_n$. Each pulse is immediately followed by free evolution of the quantum system for duration $\tau_1, \dots, \tau_n$, respectively. With each applied pulse, an initial Hamiltonian H_0 is rotated to be

$$H_i = (P_i \cdots P_1)^\dagger H_0 (P_i \cdots P_1), \tag{1}$$

such that state evolution during the ith free evolution frame is given by the piecewise constant Hamiltonian H_i. For a total sequence duration $t = \tau_1 + \tau_2 + \cdots + \tau_n$, AHT approximates the unitary propagator [30] as $\mathcal{U}^{(m)}(t) = \exp(-i\mathcal{H}^{(m)}t)$, where $\mathcal{H}^{(m)}$ denotes a time-independent effective Hamiltonian described by the Magnus expansion, $\mathcal{H}^{(m)} = \bar{H}^{(1)} + \cdots + \bar{H}^{(m)}$. For reference, the first two terms in the expansion are provided in Eq. (2). The first-order contribution $\bar{H}^{(1)}$ describes the mean of the interaction frame Hamiltonians H_i, weighted by the duration of each corresponding free evolution interval τ_i. Higher-order terms consist of summations over increasing numbers of nested commutators.

$$\bar{H}^{(1)} = \frac{1}{t}\sum_i^n H_i\tau_i, \;\; \bar{H}^{(2)} = \frac{1}{2t}\sum_{j=1}^n\sum_{i=1}^{j-1}[H_j, H_i]\tau_j\tau_i. \tag{2}$$

If the sequence is repeated, then t is the duration of a single Floquet cycle with $\mathcal{H}^{(m)}$ remaining unchanged. The total propagator is obtained by applying $\mathcal{U}^{(m)}(t)$ once for each cycle.

III. AHT BREAKDOWN

To characterize the effect of a specific pulse sequence on sensor performance, we define the sensor coupling factor $\gamma = \partial\Delta/\partial V$, which represents a first-order shift in the sensor energy level difference Δ with respect to a target (classical) signal field V to be measured [31]. Sensitivity to changes in V scales linearly with respect to γ, roughly following $\eta \propto \frac{1}{\gamma\sqrt{T_d}}$, where T_d refers to the characteristic timescale over which a measurement observable decays (e.g., due to dephasing or decoherence).

For accurate assessments of sensitivity, reliable estimates of γ are crucial. For example, when using electronic spins for magnetic field measurements, γ represents an "effective" gyromagnetic ratio and can be defined with respect to the electron gyromagnetic ratio $\gamma_e \approx -2.8 \times 10^{10}$ Hz/T. We therefore introduce a dimensionless coupling factor $\alpha = \gamma/\gamma_e$, which represents a suppression of the bare electron response that depends on the sensing protocol employed. In other words, α is fixed for a given sensing protocol, even if the sensor platform (e.g., electronic spins) is changed.

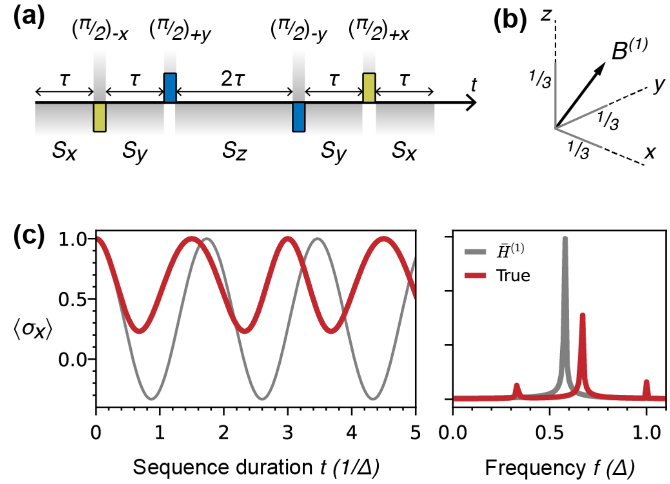

FIG. 1. (a) WAHUHA pulse sequence and toggling frame representations. (b) Effective field corresponding to leading-order average Hamiltonian. (c) WAHUHA time series $\langle\sigma_x(t)\rangle$ and corresponding power spectra, obtained using the first-order average Hamiltonian (gray) vs ground-truth unitary evolution (red).

Previous approaches used AHT to estimate α for a given sensing protocol [20,21]. To evaluate the sensor response due to a target Hamiltonian H_0, the first-order average Hamiltonian $\mathcal{H}^{(1)}$ is projected onto the relevant basis operators, e.g., the spin operators S_x, S_y, S_z. The components of α (normalized by H_0) are calculated using

$$a_{x,y,z} = \frac{\sqrt{2}\mathrm{Tr}(\mathcal{H}^\dagger S_{x,y,z})}{\sqrt{\mathrm{Tr}(H_0^\dagger H_0)}}, \tag{3}$$

such that $\alpha = \sqrt{a_x^2 + a_y^2 + a_z^2}$. Note that this requires $\mathcal{H}$ to be linear with the spin operators.

To provide intuition for α, we consider the highly influential WAHUHA pulse sequence, which was originally conceived by Waugh *et al.* [32] to decouple homonuclear magnetic dipolar interactions in solid-state NMR. As shown in Fig. 1(a), the WAHUHA protocol consists of four $\pi/2$-rotation pulses applied along $-S_x, S_y, -S_y, S_x$, with pulse delays proportional to τ. By spending equal time along orthogonal field directions, WAHUHA generates a vanishing first-order average Hamiltonian $\bar{H}^{(1)} = 0$ for spins coupled by dipolar interactions.

Applying WAHUHA to a target magnetic field $\vec{B}_0 = B_0\hat{z}$ such that $H_0 = -\gamma_e B_0 S_z$, Eq. (2) reveals the first-order average Hamiltonian,

$$\mathcal{H}^{(1)} = -\gamma_e\frac{B_0}{3}(S_x + S_y + S_z). \tag{4}$$

Here, $\mathcal{H}^{(1)}$ is described by an effective field $\vec{B}^{(1)} = (B_0/3, B_0/3, B_0/3)$, as illustrated in Fig. 1(b). Setting $\mathcal{H} = \mathcal{H}^{(1)}$ in Eq. (3) results in $\alpha = |\vec{B}^{(1)}|/|\vec{B}_0| = 1/\sqrt{3}$. Indeed, α denotes the fractional length of the effective field associated with $\mathcal{H}$, relative to the corresponding field of the target Hamiltonian H_0 [33].

The leading-order result in Eq. (4) predicts state precession around the effective field $\vec{B}^{(1)}$ with a single-tone frequency $\Delta/\sqrt{3}$, where $H_0 = \Delta S_z$. In Fig. 1(c), we show the resulting spin dynamics due to $\mathcal{U}^{(1)}$ and compare to the time evolution using the exact unitary,

$$U_0 = (e^{-iH_0\tau_n}P_n)\cdots(e^{-iH_0\tau_2}P_2)(e^{-iH_0\tau_1}P_1). \tag{5}$$

Here, we assume instantaneous pulses applied to an initial state prepared along S_x. The time-dependent state projection onto S_x is plotted as a function of time t, evolved separately using unitaries $\mathcal{U}^{(1)}$ (gray curve) and U_0 (red curve). Immediately, we observe significant differences. In contrast to the single frequency oscillation $\Delta/\sqrt{3}$ predicted by $\bar{H}^{(1)}$, the true time series exhibits beatings with multiple tones, with none at the frequency $\Delta/\sqrt{3}$. This behavior is also clearly seen in the accompanying power spectra in Fig. 1(c). The amplitude of the WAHUHA fringes also greatly differs from AHT predictions.

Magnus expansion convergence. Typically, sufficient conditions for convergence of the Magnus expansion are established using a radius of convergence r_c [6,7],

$$\sum_i^n |H_i|\tau_i < \frac{r_c}{2\pi}, \tag{6}$$

where $|\cdots|$ represents the spectral norm. The pulses generate piecewise constant Hamiltonians during each free evolution interval, and the spectral norm $|H_i| = \Delta/2$ remains unchanged. Using the upper bound $r_c \approx 1.087$ from Refs. [35,36], the condition in Eq. (6) simplifies to

$$\Delta \times t < \frac{r_c}{\pi} \approx 0.346. \tag{7}$$

To guarantee convergence, the energy scale Δ of the interaction frame Hamiltonian and the total sequence duration t can be chosen so that their product does not exceed this threshold [37]. Although Eq. (7) assures convergence for the series expansion as a whole, it is common practice to truncate the series to the first few terms due to the increasing complexity of higher-order Magnus terms. Despite truncation, our analysis of low-order WAHUHA contributions shows clear signs of AHT breakdown near this threshold, as detailed in Appendix A.

With these results in mind, we consider the typical operating regime for sensing, with NV centers in diamond as an example. At both low and high defect densities (where dipolar spin interactions start to be prominent), local magnetic disorder forms the dominant contribution to the NV Hamiltonian [38]. Spin resonance linewidths can range from $\sim 10^4$ Hz to upward of 10^6 Hz, which inform the typical magnitude of observable changes in Δ. Moreover, the presence of NV hyperfine interactions with both onboard nitrogen and neighboring ^{13}C nuclear spins in the diamond lattice often result in additional 10^6 Hz-scale frequency detunings during control pulses. Optimal sequence durations t for sensing are typically limited by dephasing/decoherence times that frequently exceed 10^{-6} s. In short, pulsed sensing experiments in these systems routinely operate in a regime where Magnus series convergence is not guaranteed, and AHT convergence is mainly limited by single-qubit contributions.

IV. EXACT SENSOR COUPLING FACTOR

Considering the limitations of AHT convergence, we propose a method to calculate the exact (dimensionless) coupling factor, denoted here as α_ϵ. First, we consider deviations from the ground-truth unitary evolution by introducing a perturbation field V (i.e., a target signal field to be measured) to the internal Hamiltonian H_0 in Eq. (5). The resulting unitary evolution operator is given by

$$U_1 = (e^{-i(H_0+V_n)\tau_n}P_n)\cdots(e^{-i(H_0+V_1)\tau_1}P_1). \tag{8}$$

We choose V to be a small static (dc) perturbation field such that $V_k = \epsilon S_z$, with ϵ as a tunable scalar coefficient. Next, we define U_ϵ such that $U_1 = U_\epsilon U_0$, or equivalently,

$$U_\epsilon = U_1 U_0^\dagger. \tag{9}$$

Note that $U_1 = U_0$ in the absence of a signal field ($\epsilon = 0$), reducing U_ϵ to the identity operator. Therefore, any nontrivial rotation generated by U_ϵ is due to a nonzero signal contribution from V.

Since U_ϵ is unitary, it can be expressed as $U_\epsilon = e^{-i\Omega(t)}$, where $\Omega(t)$ denotes an effective time-dependent operator to be determined. After diagonalizing U_ϵ to $\mathcal{D}(t) = \mathcal{P}^{-1}U_\epsilon\mathcal{P}$, we evaluate the principal logarithm of its eigenvalues along the diagonal of $\mathcal{D}(t)$ to obtain

$$\Omega(t) = i\mathcal{P}\log[\mathcal{D}(t)]\mathcal{P}^{-1}. \tag{10}$$

To ensure that $\Omega(t)$ represents the perturbative response, it is necessary to tune ϵ, for example, by ensuring $|\epsilon t| \ll 1$ [39]. In line with AHT, we then extract an effective Hamiltonian H_ϵ by setting $\Omega(t) = H_\epsilon t$ but allow H_ϵ to retain a functional dependence on the sequence duration t. After normalizing the projection of $H_\epsilon(t)$ with respect to the perturbation, we obtain the exact coupling factor

$$\alpha_\epsilon(t) = \frac{\sqrt{2\sum_{i\in\{x,y,z\}}\mathrm{Tr}(H_\epsilon^\dagger S_i)^2}}{\sqrt{|\mathrm{Tr}(V^\dagger V)|}}. \tag{11}$$

By isolating the influence of the perturbation ϵ, this approach obtains the effective Hamiltonian due to a signal response beyond AHT. In general, this is not possible using solely AHT (even at higher expansion orders) due to its lack of convergence.

As a check, we apply this method to a Ramsey sequence, which consists of a single toggling frame Hamiltonian $H_1 = S_z$. In this case, Eq. (8) simplifies to $U_\epsilon = e^{-i(S_z+\epsilon S_z)\tau}e^{+i(S_z)\tau} = e^{-i\epsilon S_z\tau}$ to reveal the effective Hamiltonian $H_\epsilon(t) = \epsilon S_z$, resulting in an exact coupling factor of $\alpha_\epsilon = 1$ that agrees with AHT.

For the WAHUHA sequence, we plot $\alpha_\epsilon(t)$ as a function of sequence duration t in Fig. 2, along with individual projections along S_x, S_y, S_z, for a nonzero initial detuning of 1 MHz. First, we note that $\alpha_\epsilon(t) = 1/\sqrt{3}$ as the sequence duration approaches zero, agreeing with leading-order AHT for

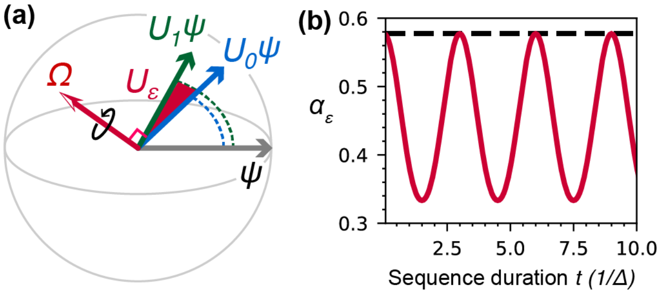

FIG. 2. (a) An initial state ψ is transformed by a pulse sequence unitary propagator to $U_0\psi$. In the presence of a perturbation field V (i.e., a target signal field to be measured), the final state is $U_1\psi$. The operator Ω generates a unitary operator $U_\epsilon = e^{-i\Omega(t)}$ such that $U_1 = U_\epsilon U_0$. (b) Exact coupling factor α_ϵ for the WAHUHA pulse sequence, as sequence duration t is increased.

sufficiently small timescales. However, $\alpha_\epsilon(t)$ quickly oscillates below this value, demanding careful choice of the sequence duration t for ideal performance.

V. RETAINING CONVERGENCE WITH RAPID ECHOES

We extend this method to determine α_ϵ in response to an oscillating (ac) target signal field. For simplicity, we describe the target ac field as a square wave perturbation during the free evolution intervals, as illustrated in Fig. 3(a). By substituting $V_k = (-1)^k \epsilon S_z$ into Eq. (8) and following the steps in Eqs. (9)–(11), we determine the effective time-dependent operator Ω due to this ac perturbation, and the corresponding α_ϵ.

We then apply this analysis to three pulse sequences XY8, DROID-60, and WAHUHA + Echo [19]. Their toggling frame transformations are shown in Fig. 3(a), for an initial static magnetic field along $+S_z$. All three sequences compensate each free precession interval around a given axis with an equal period in the opposite direction. Such "echo" structures generate a null first-order average Hamiltonian, $\bar{H}^{(1)} = 0$, suppressing contributions from the static field but retaining a response to the target ac magnetic field.

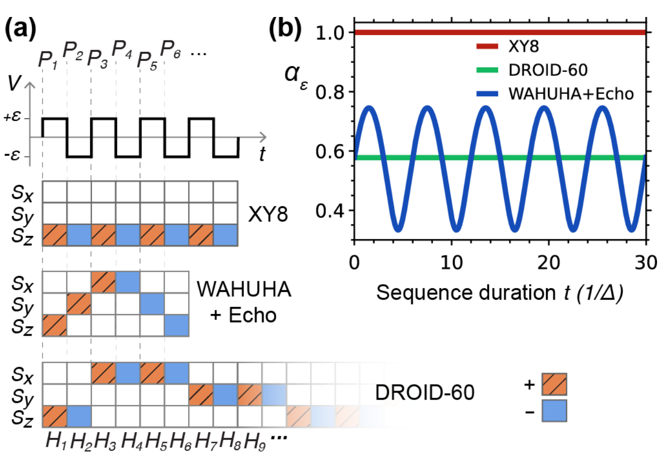

FIG. 3. (a) Square wave perturbation with amplitude ϵ, changing sign with each toggling frame. Each pulse P_i is applied to the quantum sensor (e.g., NV electronic spins in diamond) before the ith frame. For an initial sensor spin Hamiltonian S_z, the resulting toggling frame Hamiltonians for pulse sequences XY8, WAHUHA+Echo, and DROID-60 are shown. (b) For each sequence, the numerically calculated coupling factor α_ϵ is plotted as a function of sequence duration t. Calculations for XY8 and DROID-60 agree with predictions obtained from first-order AHT, i.e., $\bar{H}^{(1)}$.

In particular, XY8 and DROID-60 are commonly employed for high-sensitivity ac magnetometry in NV ensembles [22]. In the case of XY8, which consists of a regular series of π pulses, all toggling frame Hamiltonians commute ($[H_i, H_j] = 0$ for all i, j) to give $\alpha_\epsilon = 1$, analogous to the Ramsey example discussed above. In contrast, both DROID-60 and WAHUHA+Echo cycle between three orthogonal field orientations to give the first-order AHT prediction $\alpha = 1/\sqrt{3}$ in response to an ac target signal field [21]. For each sequence, the exact coupling factor α_ϵ is shown in Fig. 3(b) as a function of sequence duration. Although all three sequences retain a response to ac magnetic fields, only AHT predictions for XY8 and DROID-60 align with the exact calculation ($\alpha_\epsilon(t) \approx \alpha$). Here, exiting the radius of convergence established in Eq. (7) does not signal a breakdown of the AHT prediction. However, WAHUHA+Echo exhibits oscillations in $\alpha_\epsilon(t)$, deviating from the predictions of AHT.

We identify a common property of XY8 and DROID-60 that ensures the accuracy of AHT beyond the radius of convergence, namely, the presence of a "rapid" echo structure. Specifically, we refer to rapid echoes as having pairs of nearest-neighbor toggling frame Hamiltonians with opposite sign, such that $H_{2l} = -H_{2l-1}$ for all positive integers l. For any sequence that obeys this rapid echo structure, we show that all Magnus expansion contributions are zero (see Supplemental Material [40]). The inclusion of a small ac signal field only introduces an $\sim(\epsilon t)^m$ contribution into each term $\bar{H}^{(m)}$; thus, the system dynamics can be effectively described using only $\bar{H}^{(1)}$.

To summarize, Hamiltonian dynamics that commute at all times (XY8 and Ramsey) and the presence of rapid spin echoes (DROID-60 and XY8) are special cases where the Magnus expansion remains accurate beyond the sufficient radius of convergence. No additional requirement is placed on such Hamiltonians, making them applicable to pulse sequences beyond those mentioned here. This includes sequences designed for multiqubit settings, where entanglement can be present and exploited.

VI. RELATIONSHIP WITH QFI

AHT is also instrumental for evaluating key figures of merit for entanglement-enhanced metrology, such as QFI [25,29,41,42]. Evaluating QFI for complex pulse sequences that encode information in the quantum state across multiple free evolutions can be a nontrivial task. If AHT converges, we find that QFI takes a closed form given by

$$\mathcal{F}_Q[|\Psi(\epsilon)\rangle] = 4t^2 \mathrm{Var}_{\Psi_1}(H), \tag{12}$$

where $\mathrm{Var}_{\Psi_1}(H)$ denotes the variance of the operator H over the state $|\Psi_1\rangle = U_0 |\Psi_0\rangle$ and $U_\epsilon = \exp(-i\epsilon H t)$ (see derivation in the Supplemental Material [40]). Thus, identifying scenarios where convergence is guaranteed—such as the aforementioned rapid echoes—shortcuts (i.e., makes more efficient) the evaluation of pulse sequences for entanglement-enhanced metrology [26,27,43,44] and benchmarking of entangled input states, $|\Psi_0\rangle$.

In Appendix B, we use our formalism to show that a squeezing echo sequence (similar to Refs. [26,27]) maps into a nonlinear interferometer [45]. Notably, the effective Hamiltonian becomes the two-axis countertwisting Hamiltonian [28]. This connection is only possible because of the convergence of AHT—a direct result of the echo structure.

VII. OUTLOOK

Recent applications of AHT range from robust dynamical decoupling and sensing protocols to engineering a wide array of Hamiltonians for probes of many-body physics [41,42]. In this work, we characterize the breakdown of AHT for approximating features of time series data and the sensor coupling factor, illustrated by example pulse sequences used for sensing with solid-state spins. We also analyze sufficient convergence criteria for the Magnus expansion for a general two-level system.

Using exact methods to determine the sensor coupling factor, we show that rapid echoes allow the Magnus approximation to remain accurate well beyond its guaranteed radius of convergence. This beyond AHT result is merely one example of structures that validate the Magnus approximation, opening up opportunities for Hamiltonian engineering principles without the increasing computational cost of higher-order Magnus expansion terms [34,46]. We also present an example where it efficiently informs sequence design for entanglement-enhanced metrology. With AHT convergence informing dynamics and calculation of key metrics such as the QFI, our results apply to multiqubit systems where entanglement plays a crucial role.

These exact methods are valid regardless of Magnus expansion convergence and are readily adapted to more complex systems and noise sources. Example contributors that dominate dephasing and decoherence in solid-state spin systems include finite pulse errors, rotation angle errors, and interacting systems. At higher defect densities, parasitic spin bath contributions are also significant [20], eventually capping sensitivity beyond a critical defect concentration [21]—warranting additional developments in interaction-decoupling protocols [25]. This high-density regime can further degrade signal contrast and coherence due to unstable charge dynamics [47–50]. In addition, frequency-domain analysis can complement existing filter function approaches, frequently employed to study dynamical decoupling protocols across quantum information science [51–53]. We foresee future use of beyond AHT techniques in designing optimized measurement protocols that adhere to leading-order Magnus approximations in the presence of dephasing sources, and as potential reward metrics for optimal control and machine learning approaches [20,54,55]. Extending this beyond AHT approach to higher-dimensional systems may also be relevant to sensing protocols that leverage qudit structures [25,56,57]. However, in such cases we expect the contributions to the radius of convergence in Eq. (7) to remain pertinent.

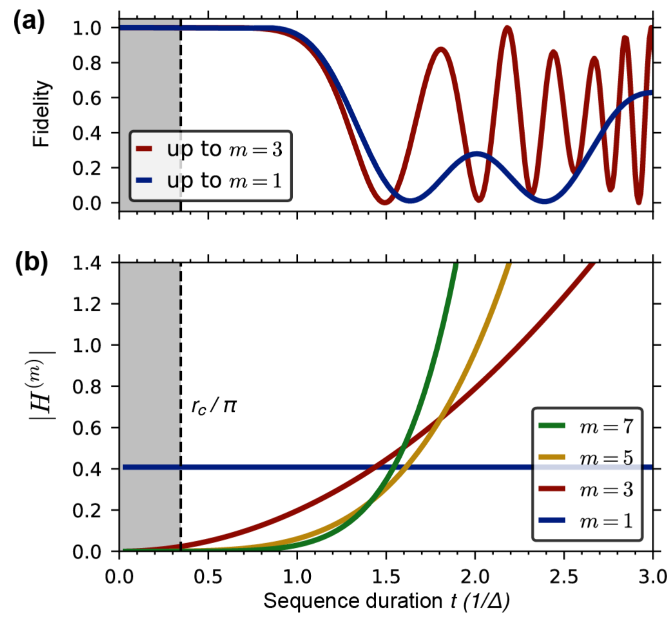

FIG. 4. (a) State fidelity comparison between exact and AHT evolution for varying sequence duration t, where $\mathcal{U}^m(t)$ is calculated for $m = 1, 3$ and compared to the ground-truth unitary $U_0(t)$. (b) Spectral norm of Magnus expansion terms $|\bar{H}^m|$ for $m = 1, 3, 5, 7$ for the WAHUHA protocol, for varying sequence duration t. The region of guaranteed Magnus series convergence $t < r_c/\pi$ is shaded in gray.

ACKNOWLEDGMENTS

We gratefully acknowledge Hengyun Zhou and Haoyang Gao for helpful discussions. This work was supported by, or in part by, the DEVCOM Army Research Laboratory under Contract No. W911NF1920181 and under Cooperative Agreement No. W911NF-24-2-0044 (S.C.C.); the DEVCOM ARL Army Research Office under Grant No. W911NF2120110; the U.S. Air Force Office of Scientific Research under Grant No. FA9550-22-1-0312; and the University of Maryland Quantum Technology Center.

DATA AVAILABILITY

The data that support the findings of this study are available from the corresponding author upon reasonable request.

APPENDIX A: AHT CONVERGENCE IN WAHUHA

To investigate the discrepancy between the AHT prediction of time evolution and the exact dynamics in WAHUHA, we include higher-order contributions to calculate $\mathcal{U}^{(m)}$, for the same target Hamiltonian and initial state $|+x\rangle$ as in the main text. Figure 4(a) shows a comparison of state fidelity between exact and AHT evolution [58]. Notably, as the sequence length t is extended, $\mathcal{U}^{(3)}$ produces fringes with increasing precession frequency, which suggests that the energy scale of $\bar{H}^{(3)}$ is increasing with time t. This observation prompts us in the main text to consider the conditions where the Magnus expansion is expected to be valid.

As stated in the main text, Eq. (7) assures convergence for the series expansion as a whole and it is common practice to truncate the series to the first few terms due to the increasing computational complexity of calculating higher-order terms of the expansion. To compare the relative contributions from these leading terms, the spectral norms $|\bar{H}^{(m)}|$ for the WAHUHA sequence are plotted in Fig. 4(b) as a function of sequence duration t, for m up to 7 [40,59]. As expected from Eq. (2), $|\bar{H}^{(1)}|$ is constant with respect to the sequence duration t, since the weighted average of the toggling frame Hamiltonians is unchanged. However, the norms of higher-order contributions increase with t, and eventually dominate. Specifically, we observe that $|\bar{H}^{(m)}| \propto (\Delta \cdot t)^{m-1}$, which follows from the m nested summations (or more generally, time integrals) that are present in $\bar{H}^{(m)}$.

APPENDIX B: APPLICATION TO ENTANGLEMENT-ENHANCED SENSING

As an illustration of applications of our results outside the realm of dynamical decoupling, we consider a squeezing echo sequence (similar to Refs. [26,27] or a Loschmidt echo [60]) where $H_1 = \chi S_z^2$ and $H_2 = -\chi S_z^2$, a time-reversal application of one-axis twisting. If there is an extra bias field ϵS_y, the effective Hamiltonian becomes $H_{\text{eff}} = \epsilon S_y + \epsilon\tau H_{\text{TACT}}$ where $H_{\text{TACT}} = \chi[(S_z + S_x)^2 + (S_z - S_x)^2]/2$ is a two-axis countertwisting Hamiltonian (over an axis rotated by $\pi/4$). This result reveals a hidden connection between a time-reversal application of one-axis twisting and the two-axis countertwisting. Interestingly, the squeezing echo behaves like a nonlinear interferometer capable of providing Heisenberg limit scaling (the maximum theoretical sensitivity scaling where QFI scales as N^2) with a coherent state as input [45]. We provide more details in the Supplemental Material [40]. We note that this connection is only possible because of the convergence of AHT, a result of the echo structure. Alternatively, one could also understand this echo sequence as a way to amplify small perturbations [26,27], just as a Loschmidt echo is often understood [60]. These interpretations are complementary and complete the picture discussed here.

[1] W. Magnus, On the exponential solution of differential equations for a linear operator, Commun. Pure Appl. Math. **7**, 649 (1954).

[2] J. A. Oteo and J. Ros, The Magnus expansion for classical Hamiltonian systems, J. Phys. A: Math. Gen. **24**, 5751 (1991).

[3] A. Connes and D. Kreimer, Renormalization in quantum field theory and the Riemann-Hilbert problem I: The Hopf algebra structure of graphs and the main theorem, Commun. Math. Phys. **210**, 249 (2000).

[4] D. W. Robinson, Multiple Coulomb excitations of deformed nuclei, Helv. Phys. Acta (Switzerland) **36**, 140 (1963).

[5] J. Eichler, Magnus approximation for K-shell ionization by heavy-ion impact, Phys. Rev. A **15**, 1856 (1977).

[6] S. Blanes, F. Casas, J. Oteo, and J. Ros, The Magnus expansion and some of its applications, Phys. Rep. **470**, 151 (2009).

[7] F. Casas, Sufficient conditions for the convergence of the Magnus expansion, J. Phys. A: Math. Theor. **40**, 15001 (2007).

[8] A. Brinkmann, Introduction to average Hamiltonian theory. I. Basics, Concepts Magn. Reson. **45A**, e21414 (2016).

[9] W. Evans, On some applications of the Magnus expansion in nuclear magnetic resonance, Ann. Phys. (NY) **48**, 72 (1968).

[10] U. Haeberlen and J. S. Waugh, Coherent averaging effects in magnetic resonance, Phys. Rev. **175**, 453 (1968).

[11] M. Edén and M. H. Levitt, Pulse sequence symmetries in the nuclear magnetic resonance of spinning solids: Application to heteronuclear decoupling, J. Chem. Phys. **111**, 1511 (1999).

[12] M. Goldman, P. J. Grandinetti, A. Llor, Z. Olejniczak, J. R. Sachleben, and J. W. Zwanziger, Theoretical aspects of higher-order truncations in solid-state nuclear magnetic resonance, J. Chem. Phys. **97**, 8947 (1992).

[13] E. S. Mananga and T. Charpentier, Introduction of the Floquet-Magnus expansion in solid-state nuclear magnetic resonance spectroscopy, J. Chem. Phys. **135**, 044109 (2011).

[14] D. Candoli, I. K. Nikolov, L. Z. Brito, S. Carr, S. Sanna, and V. F. Mitrović, Pulsee: A software for the quantum simulation of an extensive set of magnetic resonance observables, Comput. Phys. Commun. **284**, 108598 (2023).

[15] S. C. Carrasco, S. Lourette, I. Sola, and V. S. Malinovsky, Dynamically enhanced two-photon spectroscopy, Phys. Rev. Lett. **134**, 163601 (2025).

[16] O. Sahin, E. de Leon Sanchez, S. Conti, A. Akkiraju, P. Reshetikhin, E. Druga, A. Aggarwal, B. Gilbert, S. Bhave, and A. Ajoy, High field magnetometry with hyperpolarized nuclear spins, Nat. Commun. **13**, 5486 (2022).

[17] P. Balasubramanian, C. Osterkamp, Y. Chen, X. Chen, T. Teraji, E. Wu, B. Naydenov, and F. Jelezko, DC magnetometry with engineered nitrogen-vacancy spin ensembles in diamond, Nano Lett. **19**, 6681 (2019).

[18] S. Choi, N. Y. Yao, and M. D. Lukin, Dynamical engineering of interactions in qudit ensembles, Phys. Rev. Lett. **119**, 183603 (2017).

[19] J. Choi, H. Zhou, H. S. Knowles, R. Landig, S. Choi, and M. D. Lukin, Robust dynamic Hamiltonian engineering of many-body spin systems, Phys. Rev. X **10**, 031002 (2020).

[20] M. F. O'Keeffe, L. Horesh, J. F. Barry, D. A. Braje, and I. L. Chuang, Hamiltonian engineering with constrained optimization for quantum sensing and control, New J. Phys. **21**, 023015 (2019).

[21] H. Zhou, J. Choi, S. Choi, R. Landig, A. M. Douglas, J. Isoya, F. Jelezko, S. Onoda, H. Sumiya, P. Cappellaro, H. S. Knowles, H. Park, and M. D. Lukin, Quantum metrology with strongly interacting spin systems, Phys. Rev. X **10**, 031003 (2020).

[22] N. Arunkumar, K. S. Olsson, J. T. Oon, C. A. Hart, D. B. Bucher, D. R. Glenn, M. D. Lukin, H. Park, D. Ham, and R. L. Walsworth, Quantum logic enhanced sensing in solid-state spin ensembles, Phys. Rev. Lett. **131**, 100801 (2023).

[23] K. Khodjasteh and D. A. Lidar, Performance of deterministic dynamical decoupling schemes: Concatenated and periodic pulse sequences, Phys. Rev. A **75**, 062310 (2007).

[24] G. S. Uhrig, Keeping a quantum bit alive by optimized π-pulse sequences, Phys. Rev. Lett. **98**, 100504 (2007).

[25] H. Zhou, L. S. Martin, M. Tyler, O. Makarova, N. Leitao, H. Park, and M. D. Lukin, Robust higher-order Hamiltonian engineering for quantum sensing with strongly interacting systems, Phys. Rev. Lett. **131**, 220803 (2023).
[26] O. Hosten, R. Krishnakumar, N. J. Engelsen, and M. A. Kasevich, Quantum phase magnification, Science **352**, 1552 (2016).
[27] S. Colombo, E. Pedrozo-Peñafiel, A. F. Adiyatullin, Z. Li, E. Mendez, C. Shu, and V. Vuletić, Time-reversal-based quantum metrology with many-body entangled states, Nat. Phys. **18**, 925 (2022).
[28] M. Kitagawa and M. Ueda, Squeezed spin states, Phys. Rev. A **47**, 5138 (1993).
[29] S. L. Braunstein and C. M. Caves, Statistical distance and the geometry of quantum states, Phys. Rev. Lett. **72**, 3439 (1994).
[30] Multiplicative factors of the reduced Planck constant $\hbar$ are dropped in the exponent for simplicity. All Hamiltonian operators have nonangular frequency units in this work.
[31] C. L. Degen, F. Reinhard, and P. Cappellaro, Quantum sensing, Rev. Mod. Phys. **89**, 035002 (2017).
[32] J. S. Waugh, L. M. Huber, and U. Haeberlen, Approach to high-resolution NMR in solids, Phys. Rev. Lett. **20**, 180 (1968).
[33] Alternatively, Ref. [34] calculates α by considering the largest difference between the eigenvalues of $\bar{H}^{(1)}$, giving the same result for a two-level system.
[34] H. Zhou, H. Gao, N. T. Leitao, O. Makarova, I. Cong, A. M. Douglas, L. S. Martin, and M. D. Lukin, Robust Hamiltonian engineering for interacting qudit systems, Phys. Rev. X **14**, 031017 (2024).
[35] S. Blanes, F. Casas, J. A. Oteo, and J. Ros, Magnus and Fer expansions for matrix differential equations: The convergence problem, J. Phys. A: Math. Gen. **31**, 259 (1998).
[36] P. C. Moan and E. Ew, Efficient approximation of Sturm-Liouville problems using Lie-group methods, Technical Report No. 1998/NA11, University of Cambridge, Cambridge, United Kingdom, 1999.
[37] Alternately, one could prevent crossing this threshold by increasing the number of Floquet cycles n_c to minimize t, while maintaining the total interferometric time, $n_c t$.
[38] G. Kucsko, S. Choi, J. Choi, P. C. Maurer, H. Zhou, R. Landig, H. Sumiya, S. Onoda, J. Isoya, F. Jelezko, E. Demler, N. Y. Yao, and M. D. Lukin, Critical thermalization of a disordered dipolar spin system in diamond, Phys. Rev. Lett. **121**, 023601 (2018).
[39] N. J. Higham, *Functions of Matrices: Theory and Computation* (Society for Industrial and Applied Mathematics, Philadelphia, 2008).
[40] See Supplemental Material at http://link.aps.org/supplemental/10.1103/w2sf-zxdk for additional details.
[41] L. S. Martin, H. Zhou, N. T. Leitao, N. Maskara, O. Makarova, H. Gao, Q.-Z. Zhu, M. Park, M. Tyler, H. Park, S. Choi, and M. D. Lukin, Controlling local thermalization dynamics in a Floquet-engineered dipolar ensemble, Phys. Rev. Lett. **130**, 210403 (2023).
[42] M. Lei, R. Fukumori, C.-J. Wu, E. Barnes, S. E. Economou, J. Choi, and A. Faraon, Quantum thermalization and Floquet engineering in a spin ensemble with a clock transition, Nat. Phys. **21**, 1196 (2025).
[43] S. C. Carrasco, M. H. Goerz, Z. Li, S. Colombo, V. Vuletić, and V. S. Malinovsky, Extreme spin squeezing via optimized one-axis twisting and rotations, Phys. Rev. Appl. **17**, 064050 (2022).
[44] S. C. Carrasco, M. H. Goerz, S. A. Malinovskaya, V. Vuletić, W. P. Schleich, and V. S. Malinovsky, Dicke state generation and extreme spin squeezing via rapid adiabatic passage, Phys. Rev. Lett. **132**, 153603 (2024).
[45] S. Boixo, S. T. Flammia, C. M. Caves, and J. M. Geremia, Generalized limits for single-parameter quantum estimation, Phys. Rev. Lett. **98**, 090401 (2007).
[46] M. Tyler, H. Zhou, L. S. Martin, N. Leitao, and M. D. Lukin, Higher-order methods for Hamiltonian engineering pulse sequence design, Phys. Rev. A **108**, 062602 (2023).
[47] X.-D. Chen, C.-L. Zou, F.-W. Sun, and G.-C. Guo, Optical manipulation of the charge state of nitrogen-vacancy center in diamond, Appl. Phys. Lett. **103**, 013112 (2013).
[48] P. Ji and M. V. G. Dutt, Charge state dynamics of the nitrogen vacancy center in diamond under 1064-nm laser excitation, Phys. Rev. B **94**, 024101 (2016).
[49] S. Dhomkar, H. Jayakumar, P. R. Zangara, and C. A. Meriles, Charge dynamics in near-surface, variable-density ensembles of nitrogen-vacancy centers in diamond, Nano Lett. **18**, 4046 (2018).
[50] I. C. Barbosa, J. Gutsche, and A. Widera, Impact of charge conversion on NV-center relaxometry, Phys. Rev. B **108**, 075411 (2023).
[51] Ł. Cywiński, R. M. Lutchyn, C. P. Nave, and S. Das Sarma, How to enhance dephasing time in superconducting qubits, Phys. Rev. B **77**, 174509 (2008).
[52] G. S. Uhrig, Exact results on dynamical decoupling by π pulses in quantum information processes, New J. Phys. **10**, 083024 (2008).
[53] M. J. Biercuk, H. Uys, A. P. VanDevender, N. Shiga, W. M. Itano, and J. J. Bollinger, Optimized dynamical decoupling in a model quantum memory, Nature (London) **458**, 996 (2009).
[54] F. Poggiali, P. Cappellaro, and N. Fabbri, Optimal control for one-qubit quantum sensing, Phys. Rev. X **8**, 021059 (2018).
[55] P. Peng, X. Huang, C. Yin, L. Joseph, C. Ramanathan, and P. Cappellaro, Deep reinforcement learning for quantum Hamiltonian engineering, Phys. Rev. Appl. **18**, 024033 (2022).
[56] H. J. Mamin, M. H. Sherwood, M. Kim, C. T. Rettner, K. Ohno, D. D. Awschalom, and D. Rugar, Multipulse double-quantum magnetometry with near-surface nitrogen-vacancy centers, Phys. Rev. Lett. **113**, 030803 (2014).
[57] C. A. Hart, J. M. Schloss, M. J. Turner, P. J. Scheidegger, E. Bauch, and R. L. Walsworth, N $-$ V-diamond magnetic microscopy using a double quantum 4-Ramsey protocol, Phys. Rev. Appl. **15**, 044020 (2021).
[58] R. Jozsa, Fidelity for mixed quantum states, J. Mod. Opt. **41**, 2315 (1994).
[59] A. Arnal, F. Casas, and C. Chiralt, A general formula for the Magnus expansion in terms of iterated integrals of right-nested commutators, J. Phys. Commun. **2**, 035024 (2018).
[60] T. Macrì, A. Smerzi, and L. Pezzè, Loschmidt echo for quantum metrology, Phys. Rev. A **94**, 010102(R) (2016).